Liquid–Liquid Phase Transitions in Tetrahedrally Coordinated Fluids via Wertheim Theory

Frank Smallenburg,*,[†] Laura Filion,[‡] and Francesco Sciortino[†]

[†]Department of Physics, Sapienza, Universitá di Roma, Piazzale Aldo Moro 2, I-00185 Roma, Italy

[‡]Soft Condensed Matter, Debye Institute for Nanomaterials Science, Utrecht University, Princetonplein 5, Utrecht 3584 CC, The Netherlands

ABSTRACT: Network interpenetration has been proposed as a mechanism for generating liquid–liquid phase transitions in one component systems. We introduce a model of four coordinated particles, which explicitly treats the system as a mixture of two interacting interpenetrating networks that can freely exchange particles. This model can be solved within Wertheim's theory for associating fluids and shows liquid–liquid phase separations (in addition to the gas–liquid) for a wide range of model parameters. We find that originating a liquid–liquid transition requires a small degree of interpenetrability and a preference for intranetwork bonding. Physically, these requirements can be seen as controlling the softness of the particle–particle interaction and the bond flexibility, in full agreement with recent findings [Smallenburg, F.; Filion, L.; Sciortino, F. *Nat. Phys.* **2014**, *10*, 653].
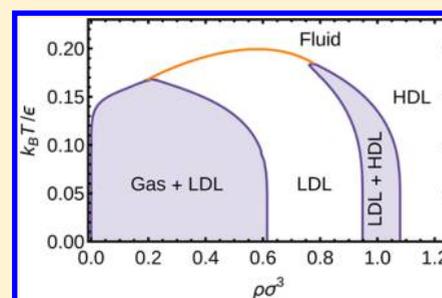
INTRODUCTION

One of the more controversial topics in liquid-state theory is the postulated presence (or conversely, lack) of a metastable liquid–liquid critical point in tetrahedrally coordinated systems, such as water, silica, silicon, and carbon.[1−9] According to this hypothesis, two different liquid phases differing in density appear at low temperature T. The existence of such a liquid–liquid (LL) transition ending in a critical point has been hypothesized as the reason for many of the thermodynamic anomalies observed in the liquid phases of these systems, including extrema in the density, isothermal compressibility, and isobaric heat capacity. However, spontaneous crystallization and slow dynamics in the region where the LL critical point is expected makes study of this phenomenon very difficult, both via experiments[7,10−13] as well as computer simulations.[14]

Over the past decade, patchy-particle models have been used extensively to study tetrahedral liquids.[15−24] These simplified models have been shown to exhibit behavior that is similar to molecular and atomic tetrahedrally coordinated liquids. Moreover, a variation on these models displays a thermodynamically stable liquid–liquid phase transition.[21] One of the more successful theoretical tools for studying liquid states in patchy systems is Wertheim theory.[25−27] This thermodynamic perturbation theory provides expressions for the free energy of associating liquids by treating the bonding as a perturbation on a nonbonding reference system, such as a hard sphere fluid. As a result, Wertheim theory does not take into account any changes in the structure of the liquid that result from forming bonds. Nonetheless, the gas–liquid phase behavior predicted by Wertheim theory has been shown to be in good agreement with simulations[28,29] and experiments[30] in numerous studies. Unfortunately, as Wertheim theory does not account for bond

stiffness or network interpenetration, the theory does not normally predict liquid–liquid phase transitions.

In this article, we design a simple model system for tetrahedrally coordinated liquids that is amenable for study using Wertheim theory and that can display liquid–liquid transitions. Our study is highly motivated by the models described in refs 21 and 31−33 and by previous investigations that have focused on the liquid–liquid phase transition between a low-density liquid (LDL) and a high-density liquid (HDL).[1,34] Several attempts to provide a description of the transition in terms of two competing local structures, differing in local volume, local entropy, and local energy[35−38] have been reported. In ref 31, network interpenetration was identified as a key mechanism driving LL phase separation. In contrast to the LDL, which consists of a single tetrahedral network, the HDL consists of two (or more) interpenetrating and intertwining networks of bonded particles. As a result, in the HDL, each particle has two types of neighbors in its first coordination shell: particles that it is bonded to (belonging to the same network) and particles that it is not bonded to (belonging to the other network). We attempt to incorporate this distinction in our model.

This article is organized as follows: First, we discuss the model and Wertheim theory in detail. Next, we calculate phase diagrams and show that this model predicts liquid–liquid phase separation for a wide range of parameters. We then investigate the thermodynamic anomalies, such as extrema in the density, that occur in the vicinity of the liquid–liquid critical point.

ACS Publications   © XXXX American Chemical Society

A

dx.doi.org/10.1021/jp508788m | *J. Phys. Chem. B* XXXX, XXX, XXX–XXX

Subsequently, we take a look at the behavior of the energy as a function of density, showing a minimum as is characteristic for tetrahedrally coordinated fluids. Finally, we end with a brief summary and discussion of our results.

■ MODEL SYSTEM

The thermodynamic perturbation theory developed by Wertheim[25−27] has proven to be an extremely useful tool for predicting and understanding the phase behavior of patchy particles[24,39−44] in the single bond per patch limit. More recently, attempts have been put forward for extending the theory to include multiple bonds per patch.[45] In the framework of the orginal theory, a fluid of patchy particles is treated as a perturbation on an unbonded reference fluid. Hence, the Helmholtz free energy per particle $f = F/N$ of a binary mixture of N particles, at a composition x, and number density ρ is given by

$$f(x, \rho, T) = f_{ref}(x, \rho, T) + f_{bond}(x, \rho, T) \tag{1}$$

with f_{ref} the reference free energy of a nonbonding system at the same density and composition, and f_{bond} the bonding free energy.

The main goal of this work is to design a model for patchy particles that can be treated by Wertheim theory in such a way that a liquid−liquid phase transition appears naturally. Building on the idea of network interpenetration, we design the model in such a way that two networks can coexist. We label these two networks A and B and associate the particles in each of the two networks with species A and B. To allow for the exchange of particles between the two networks, we impose that particles can freely switch between species. The interaction between the particles consists of a hard-core repulsion combined with attractive patches. With regards to the hard-core repulsion, we know from earlier work that liquid−liquid phase separation is favored by systems where unbonded particles can approach each other more closely than bonded particles.[21] Thus, we choose as our reference system a mixture of hard spheres with a tunable nonadditivity, so that particles of different species can partially interpenetrate. Specifically, we assume a symmetric binary mixture of nonadditive hard spheres, where the distance of closest approach σ_{ij} between particles of species i and j is given by $\sigma_{AA} = \sigma_{BB} = \sigma$ and $\sigma_{AB} = (1 + \Delta)\sigma$, with $\Delta < 0$ the nonadditivity parameter. In designing the patchy attractions, we differentiate the three possible bonding types (AA, BB, and AB). Specifically, we assume the same energy scale ϵ for all three bonding types. However, we require that bonds preferentially form between particles in the same network, by selecting different bonding volumes between similar and dissimilar interactions. This choice is motivated by the analogy between the present and the model in ref 21. To model the entropic cost involved in connecting a particle to a particle outside its own network, the bonding volume for AB bonds $\mathcal{V}_{AB}$ is chosen smaller than that for the AA or BB bonds ($\mathcal{V}_{AA} = \mathcal{V}_{BB}$). We define $\mathcal{V}_{AB} = \alpha \mathcal{V}_{AA}$. Thus, $\alpha \approx 0$ indicates that only intranetwork bonds are allowed, while $\alpha > 0$ allows for an increasing degree of internetwork bonding. As such, α can be considered a measure for the bond flexibility. In the following calculations we pick $\mathcal{V}_{AA} = 0.00424\sigma^3$. This bonding volume corresponds in the Kern−Frenkel[46] model to an angular patch width $\cos \theta = 0.9$ and an interaction range $\delta = 0.12\sigma$. Finally, we allow particles to freely switch between

species A and B. This condition is imposed by requiring that the chemical potential $\mu_A = \mu_B$.

For the reference free energy, we use the equation of state developed by Jung et al.,[47] which provides the pressure as a function of the composition and density for $-0.5 \leq \Delta \leq 1$ (see Appendix). This reference system of nonadditive hard spheres does not exhibit a demixing phase transition at any state point for the case of negative nonadditivity ($\Delta \leq 0$) studied in this work.

The bonding free energy for a binary mixture of particles that can form up to four bonds is given by[25−27,40]

$$\beta f_{bond} = \sum_{i=A,B} x_i [4 \log X_i - 2X_i + 2] \tag{2}$$

where $x_i = N_i/N$ is the fraction of particles in the system of species i, and X_i is the probability that a patch on a particle of species i is unbonded. Following Wertheim, this probability can be calculated via the law of mass action:

$$X_i = \frac{1}{1 + \rho\sigma^3 \sum_{j=A,B} x_j X_j \Delta_{ij}} \tag{3}$$

with

$$\Delta_{ij} = \frac{1}{\sigma^3} \int_{\mathcal{V}_{ij}} g_{ij}^{ref}(\mathbf{r})[\exp(\beta\epsilon) - 1] d\mathbf{r} \tag{4}$$

Here, the integral is taken over the bonding volume $\mathcal{V}_{ij}$ of a pair of particles of species i and j, and $g_{ij}^{ref}(\mathbf{r})$ is the radial distribution function of the reference system, i.e., of a mixture of nonadditive hard spheres at the same density and composition. Thus, Δ_{ij} is function of ρ and x. To simplify our calculations, we approximate this integral by replacing the functional behavior of the reference radial distribution function by its contact value:

$$\Delta_{ij} = \frac{\mathcal{V}_{ij}}{\sigma^3} g_{ij}^{ref}(\mathbf{r}_{ij}^{contact})[\exp(\beta\epsilon) - 1] \tag{5}$$

For $g_{ij}^{ref}(\mathbf{r}_{ij}^{contact})$, we use a approximation proposed by Hamad[48] (see Appendix).

Since particles can freely switch between the A and B species, at any density ρ, the most stable homogeneous state is the state that minimizes $f(\rho,x)$ as a function of x. The resulting free energy, which is solely a function of ρ, is thus given by

$$f(\rho) = \min_x [f(\rho, x)] \tag{6}$$

We find this minimum numerically, by evaluating $f(\rho,x)$ for a range of values $x \in (0,0.5)$ (note that $f(\rho,x) = f(\rho,1-x)$ due to symmetry), and using a numerical minimization algorithm near each of the compositions that constitute a local minimum in this grid. Subsequently, the overall lowest free energy is taken. We note here that the free energy as a function of the composition is typically well-behaved and shows at most three minima (two of which are equivalent due to symmetry). As a result, finding the global minimum is straightforward.

Values of $x \approx 0$ indicate that the system is composed of a single network, while $x \approx 0.5$ indicates either two interpenetrating networks (when the energy per particle is low) or a gas of finite-size clusters (when the energy per particle is high). From $f(\rho)$, gas−liquid and liquid−liquid phase coexistences can be determined via a standard common tangent construction. Phase diagrams are calculated by finding the coexistence densities for a range of temperatures T, at fixed nonadditivity Δ and flexibility α.

B

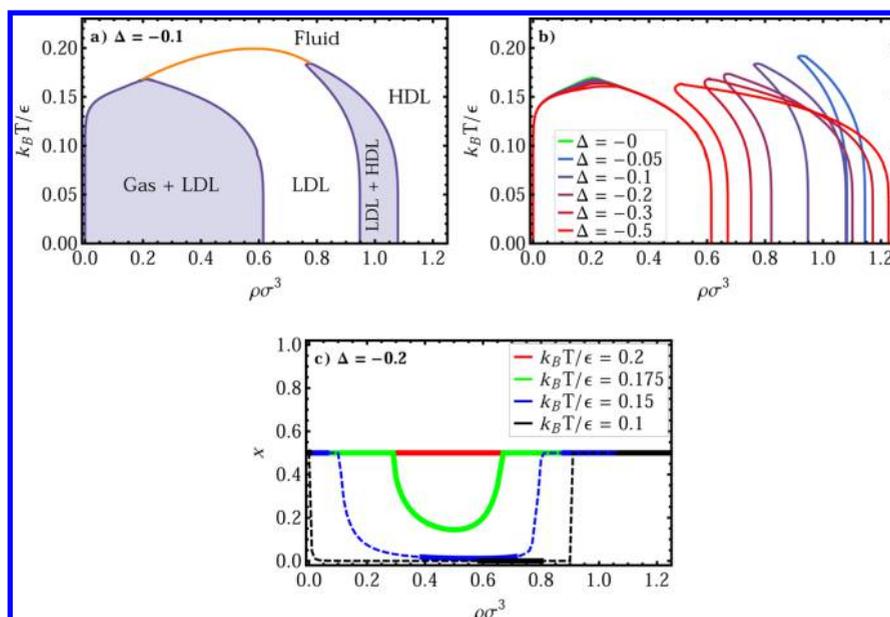dx.doi.org/10.1021/jp508788m | J. Phys. Chem. B XXXX, XXX, XXX−XXX

Figure 1. (a) Typical phase diagram for a model with no *AB*-bonding ($\alpha = 0$, $\Delta = -0.1$), including the second-order phase transition (orange line), as a function of the density ($\rho\sigma^3$) and temperature (k_BT/ϵ). Coexistence regions are colored gray, and the labels indicate the stable or coexisting phases. (b) Phase diagrams $\alpha = 0$ at different nonadditivity parameters Δ as indicated. (c) Composition as a function of density for $\Delta = -0.2$. The thinner dashed lines indicate regions where the homogeneous fluid is not the most stable phase. In these regions, the lines show the composition of the most stable homogeneous state at that density.

RESULTS AND DISCUSSION

Figure 1a,b shows phase diagrams for $\alpha = 0$, i.e., no internetwork bonding, for different negative values of the nonadditivity parameters Δ. We find that, while for $\Delta = 0$ the system displays only the standard gas—liquid coexistence, as soon as some interpenetration is allowed, a new transition appears, strongly supporting the hypothesis that softness is essential for establishing network interpenetration. We find that the gas—liquid critical point and gas—liquid coexistence curves are roughly independent of Δ. The only effect of the nonadditivity parameter on the gas—liquid transition is a slight broadening of the coexistence region at high temperatures and a slight decrease in the critical temperature T_c^{gl}. However, the novel liquid—liquid phase transition is strongly affected by changing Δ. On decreasing Δ (e.g., increasing $|\Delta|$), the liquid—liquid coexistence enters the phase diagram from the right (high density). Decreasing Δ further decreases both the LDL and HDL densities. However, the LDL coexistence density decreases much faster than the HDL one. This results in a broadening of the liquid—liquid coexistence region. Additionally, the LDL—HDL critical temperature T_c^{ll} decreases upon increasing Δ. However, the liquid—liquid critical temperature never drops below the gas—liquid critical temperature T_c^{gl} in the range where our reference free energy is valid ($\Delta \geq -0.5$). A similar behavior ($T_c^{ll} > T_c^{gl}$) was also observed in a model of particles in which the isotropic potential consists of an attractive part and two characteristic short-range repulsive distances.[49] We also find the liquid—liquid coexistence curve to be skewed to lower densities at high temperature, resulting in a re-entrant shape. Upon cooling along a constant density line, the fluid first separates and then returns to an homogeneous (LDL) phase. Such a re-entrant low density phase has been recently observed in a model of Janus colloids.[50]

Figure 1c shows the behavior of the composition along three different isotherms. At high T we always observe a fluid with mixed composition ($x \approx 0.5$). At low T the composition jumps from 0.5 in the gas phase, to zero in the LDL (indicating that this phase is indeed formed by a single network), and back again to 0.5 in the HDL, where two networks coexist. Note that in this model, states with complementary compositions x and $1 - x$ are equivalent, and therefore, the choice of either state corresponds to a spontaneous symmetry breaking. As shown by the curves in Figure 1c, the transition from a fully mixed ($x = 0.5$) to a demixed ($x \neq 0.5$) state occurs via a sharp cusp, indicating a second-order phase transition. When mapped out for different temperatures, the second-order phase transition line connects the liquid—liquid critical point to the gas—liquid coexistence curve, as shown in Figure 1a for $\Delta = -0.1$. We note here that similar behavior was observed in a mean-field lattice model for interpenetrating liquids in ref 32 as well as in other mean-field lattice models with next-nearest neighbor interactions.[51]

The second-order phase transition line is a line of critical points associated with the demixing transition in our binary model system. As a result, the liquid—liquid critical point is actually a tricritical point in our model, i.e., a point where the *A*-rich LDL, *B*-rich LDL, and HDL phases become indistinguishable. This is clearly different from the normal critical point that occurs in more typical liquid—liquid transitions (e.g., ref 21), and is a result of the artificial distinction in our model between *A*-type and *B*-type particles. Thus, both the second-order phase transition line and the tricritical nature of the liquid—liquid critical point are (as in the case of ref 32) unphysical artifacts of the model. Hence, for simplicity, we omit the second-order phase transition lines from the other ($\rho - T$) phase diagrams.

The presence of both a gas—liquid coexistence and critical demixing line, as seen in the phase diagram in Figure 1a, is reminiscent of the behavior of magnetic fluids[52,53] and symmetric binary mixtures of attractive particles.[54−57] In both of those classes of systems, a gas—liquid coexistence competes with a demixing transition, where the system changes from a

homogeneous fluid into a phase separated system of two phases characterized by either different particle species or different spin directions. Interestingly, these systems sometimes exhibit a liquid−liquid phase transition that ends in a tricritical point. This transition results from the presence of two energy scales, causing the demixed state to be energetically favored over the mixed state. In contrast, the phase diagram of the system studied here, while similar, has two important differences. First, the liquid−liquid phase transition in our model is associated with the transition from a demixed fluid to a mixed ($x = 0.5$) fluid. Second, the transition is driven by the presence of two length scales, which causes the demixed state to be entropically favored over the mixed state.

We now turn our attention to the effect of internetwork bonding (α) on the phase behavior. In Figure 2, we show phase diagrams for a range of different values of α, for $\Delta = -0.075$ and -0.125. In both cases, we see a decrease both in the LDL− HDL coexistence densities and in T_c^{ll} upon increasing α. In contrast to the behavior at $\alpha = 0$ (Figure 1), T_c^{ll} drops below T_c^{gl} for sufficiently high α. Moreover, upon increasing α even further, the critical temperature T_c^{ll} eventually decreases down to zero, and the liquid−liquid coexistence vanishes. This is accompanied by a narrowing of the coexistence region. For small degrees of interpenetration, the LDL−HDL transition always remains separate from the gas−liquid transition. For larger degrees of interpenetration (see the case $\Delta = -0.125$), before the liquid−liquid coexistence vanishes, it becomes metastable with respect to the gas−liquid coexistence. This results in a sudden broadening of the gas−liquid coexistence region, as the liquid coexisting with the gas phase is now the HDL phase. In this case, the coexisting pressure at low T becomes negative. Additionally, for sufficiently large degrees of interpenetration and internetwork bonding, the liquid−liquid transition hits the gas−liquid spinodal, and the liquid−liquid critical point becomes fully unstable (see Figure 2d).

We note here that for the case of additive hard cores (i.e., $\Delta = 0$), the liquid−liquid phase transition is absent for any choice of α. This can be understood by considering that the nonadditivity serves to favor a mixed ($x = 0.5$) state at high densities, where excluded volume effects become important. Without this nonadditivity, the system demixes upon increasing the density and never returns to $x = 0.5$, eliminating the liquid− liquid coexistence from the phase diagram. Additionally, in this case, the line of second-order phase transitions (orange line in Figure 1a) always has a positive slope.

It is now interesting to compare the behavior in Figures 1 and 2 to previous observations made regarding liquid−liquid phase transitions in tetrahedral liquids. First of all, the present results confirm that network interpenetration provides a mechanism for generating a liquid−liquid transition, as proposed in the original study of DNA tetramers.[31−33] A deeper comparison can be made to the simple tetramer model recently introduced in ref 21. This model consisted of a hard spherical core and four spherical arms with tunable flexibility and length, each decorated with a single attractive patch. Although not an exact mapping, the arm flexibility can be compared to the parameter α in our model, as arm flexibility facilitates internetwork bonding. Similarly, the arm length in ref 21 controls the closest distance of approach for two particles, analogous to our parameter Δ. For the tetramer model,[21] it was shown that upon increasing the flexibility of the arms T_c^{ll} decreases and eventually reaches 0. This is consistent with the behavior of our Wertheim theory, as shown in Figure 2. In
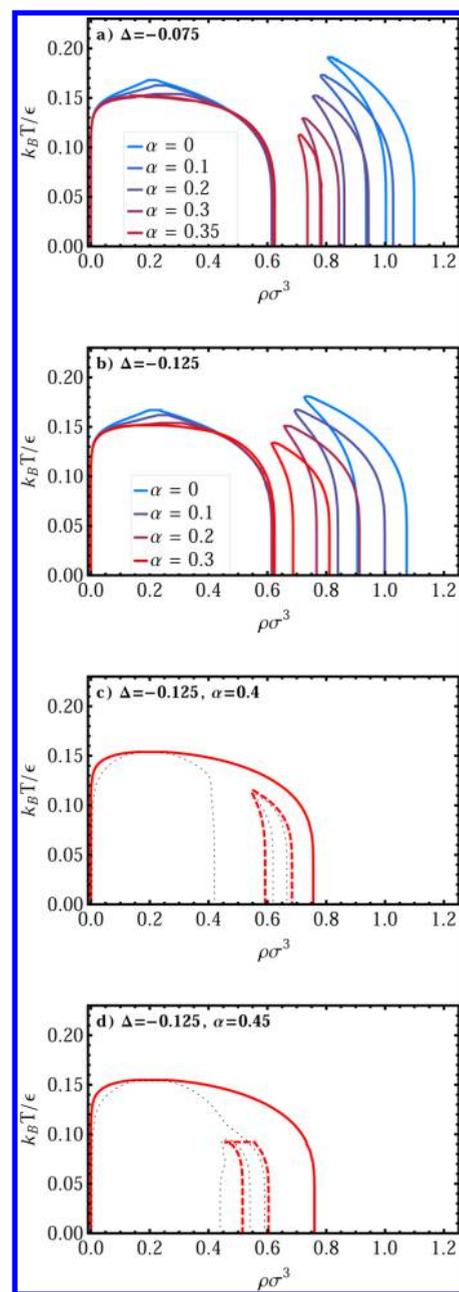

Figure 2. Phase diagrams at nonadditivity parameters $\Delta = -0.075$ (a) and $\Delta = -0.125$ (b,c), with α as indicated. For $\Delta = -0.125$, the range of α is divided up over panels (b), (c), and (d) for clarity. In panels (c) and (d), the spinodals are drawn as black dotted lines. All tie-lines are horizontal. The dashed lines indicate metastable liquid−liquid coexistences.

the tetramer model, the liquid−liquid critical temperature was shown to decrease sharply with increasing arm length. This observation is consistent with the decrease in T_c^{ll} that occurs with decreasing Δ. Additionally, in ref 21, it was also found that the density of the liquid−liquid critical point was essentially independent of the arm length (when measured in the appropriate units). This is in contrast to the model presented here, as we observe a clear decrease in critical density upon decreasing Δ.

In molecular and atomic tetrahedral liquids, the LL critical point, if present, is expected to occur at significantly lower temperature than the gas−liquid critical point. Similarly, in the

tetramer model, T_c^{ll} was always lower than T_c^{gl}.[21] In the present model, this only occurs when α is sufficiently high, i.e., when a sufficient amount of internetwork bonding is possible (see Figure 2), supporting the idea that flexibility is indeed playing a role in molecular and atomic tetrahedral liquids.

Finally, we note that the case of a negative pressure critical point, as is the case for the liquid−liquid transition in Figure 2c, has been previously proposed as a scenario for silicon.[5]

For a variety of systems, it has been shown that the presence of a liquid−liquid critical point can result in thermodynamic anomalies, which can be detected at temperatures significantly higher than T_c^{ll}. In particular, the quantities that diverge at the critical point have been shown to exhibit lines of extrema that emanate from the critical point.[58−61] Two examples are the isothermal compressibility K_T and the isobaric heat capacity C_P. Moreover, these systems have been shown to exhibit extrema in the density as a function of temperature as well. In Figure 3, we
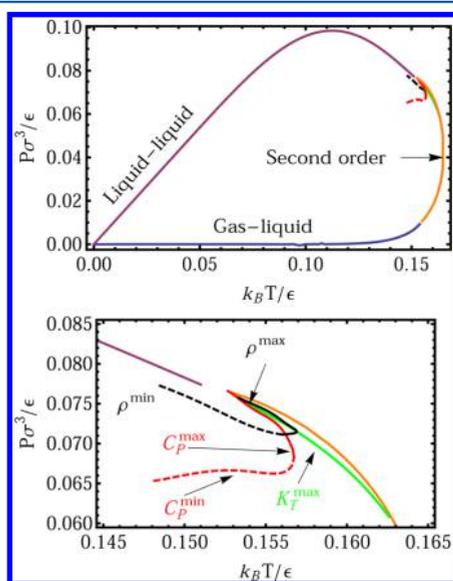

Figure 3. Phase diagrams in the $(T−P)$ representation at nonadditivity parameter $\Delta = −0.125$ and flexibility $\alpha = 0.2$. We show the coexistence lines as well as the lines of extrema in the density ρ, isothermal compressibility K_T, and isobaric heat capacity C_P. The bottom panel is a close-up of the region where these anomalies are present.

plot the extrema in K_T, C_P, and the density in the $(P−T)$ plane, together with the gas−liquid and liquid−liquid coexistence lines, for $\Delta = −0.125$ and $\alpha = 0.2$. The lines of extrema show exactly the same trends as those observed for ST2 water[59] and the tetramer model of ref 21. We note that for some choices of the parameters α and Δ, the presence of the second-order phase transition interferes with these anomalies. Interestingly, the liquid−liquid coexistence line shows a negative slope near the critical point, analogous to ST2 water. A positive slope, as the one observed in the tetramer model, is recovered at low T. The striking agreement we see between the diagrams for our Wertheim theory and ST2 suggest that this simple theoretical model is largely thermodynamically consistent with realistic models for water.

We also study the energy as a function of density for a range of temperatures, with nonadditivity parameter $\Delta = −0.3$ and flexibility $\alpha = 0.1$. Note that in this calculation we find the composition x that minimizes the free energy and determine the associated potential energy (neglecting for the time being

the possibility of phase-separation). The results for both the potential energy and the composition are shown in Figure 4.
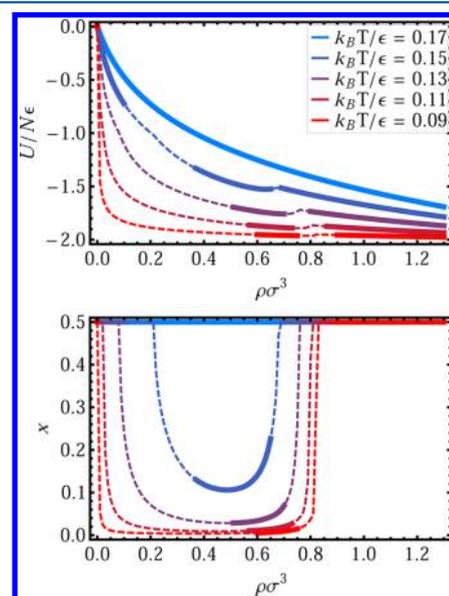

Figure 4. (top) Potential energy per particle U/N as a function of density ρ for a model with nonadditivity parameter $\Delta = −0.3$ and flexibility $\alpha = 0.1$, as a function of the density ρ. Different colors indicate different temperatures. (bottom) Composition x as a function of the density ρ for the same model. The dashed lines indicate regions where the homogeneous fluid is metastable with respect to phase separation. For this choice of model parameter the critical temperatures are $k_B T_c^{ll}/\epsilon \approx 0.165$ and $k_B T_c^{ll}/\epsilon \approx 0.155$.

Similar to previous studies on liquid−liquid phase transitions in tetrahedral systems, we see a minimum in the energy as a function of density.[62] Looking at the behavior of the composition, we observe that this minimum always occurs in the region where demixing takes place, i.e., where the composition $x \neq 0.5$. As alluded to before, we can distinguish three regimes as a function of density: (i) the gas regime, where the system consists of many clusters of both species, resulting in a composition $x = 0.5$, (ii) the liquid regime, where we see a predominance of particles of one species (either A or B), and thus $x \neq 0.5$, and (iii) the high-density liquid regime, where the composition returns to $x = 0.5$, representing two interpenetrating networks. Note that these regimes occur even above both critical temperatures. In contrast to typical observations in tetrahedral liquids, the location of the minimum in the energy is strongly dependent on T. While usually increasing density is associated with a lowering of the potential energy (due to the larger number of neighbors within the interaction range), in tetrahedral systems the increase in local density can weaken the interactions, due to distortion of the network, resulting in an optimal density at which $U(\rho)$ has a minimum.[16] Geometric constraints generated by the high directionality and fixed length of the bonds typically determine a T-independent optimal density. In the Wertheim approach, coupling between structure and bonding geometry is missing and hence such geometric constraints are not effective, resulting in shift in the minimum of $U(\rho)$ as a function of T. This is likely also related to the reentrant nature of the liquid−liquid coexistence curves, such as those in Figures 1 and 2: the density at which the LDL coexists with the HDL is typically close to the density where the potential energy is minimized. Thus, the

LDL coexistence density increases with decreasing temperature, leading to a reentrant LDL phase, which is absent in more realistic models of tetrahedral fluids.[21,31]

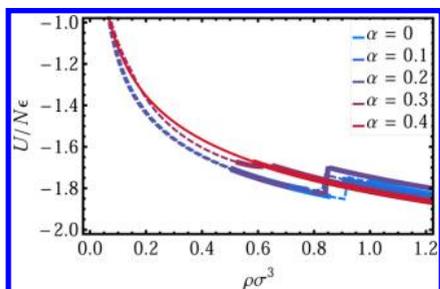In Figure 5, we compare the behavior of the energy as a function of density for systems with different degrees of

Figure 5. Potential energy per particle U/N as a function of the density ρ for a model with nonadditivity parameter $\Delta = -0.3$ and a range of internetwork bonding parameters α. For all lines, the temperature is fixed at $k_BT/\epsilon = 0.13$. The dashed lines again indicate regions where the homogeneous fluid is metastable with respect to phase separation.

internetwork bonding (i.e., different α). We note that for higher α the minimum in the energy becomes progressively less pronounced. This is consistent with the observations in the tetramer model (see Supporting Information of ref 21), where the minimum in energy was seen to become less pronounced with increasing bond flexibility. However, we note again that in the predictions in Figure 5 there is a noticeable dependence of the density at which the energy minimum takes place on α, whereas this was not observed in ref 21.

CONCLUSIONS

In conclusion, we have proposed a simple model for liquid–liquid transitions in tetrahedral fluids, which can be solved within Wertheim theory. We find good qualitative agreement between our predictions and previously studied models for tetrahedral fluids, with the exception of an additional line of second-order phase transitions. In particular, we predict liquid–liquid phase separation for a wide range of values of the interpenetrability of the particles and the internetwork bonding parameter. Furthermore, our predictions show thermodynamic anomalies around the liquid–liquid critical point that are consistent with those observed in other tetrahedral network-forming models, such as the ST2 model.[59] The minimum in potential energy as a function of density, characteristic of tetrahedral fluids, is also displayed by our model. However, the density at which this minimum occurs is strongly dependent on both the temperature and internetwork bonding parameter.

When specifically comparing our predictions with the tetramer model studied in ref 21 we see strong parallels between our internetwork bonding parameter α and the bond flexibility in the tetramer model. Upon increasing both α and the flexibility, the liquid–liquid critical temperature decreases continuously and eventually vanishes. Additionally, higher bond flexibility and high α both smoothen out the minimum in the potential energy as a function of the density.

Finally, we note that in the DNA–tetramer investigation[31] multiple liquid–liquid transitions were observed when the length of the DNA arm was sufficiently long to allow for interpenetration of more than two networks. These multiple interpenetrations could be modeled by extending the present

model to ternary (or higher order) mixtures within the Wertheim framework, simply retaining the constraint of equal chemical potential for all species.

APPENDIX: REFERENCE SYSTEM

In this Appendix, we provide the expressions used for the free energy and the contact value of the radial distribution function of our reference system; a nonadditive binary hard-sphere mixture.

To calculate the Helmholtz free energy per particle f_{ref} of a nonadditive binary mixture of hard spheres, with nonadditivity parameter Δ, total number density ρ, and composition x, we use the empirical equation of state determined by Jung et al. in ref 47. This equation of state expresses the pressure P of the system as

$$\frac{\beta P}{\rho} = 1 + \frac{4\eta(1 - c_1\eta + c_2\eta^2)}{(1 - c_3\eta + c_4\eta^2)^3} \tag{7}$$

where η is a packing fraction defined as

$$\eta = \frac{1}{4}B_2\rho \tag{8}$$

with B_2 the (analytically known) second virial coefficient of the binary mixture

$$B_2 = \frac{\pi}{3}\sigma^3[2 + 4\Delta(3 + 3\Delta + \Delta^2)x(1 - x)] \tag{9}$$

and $\sigma = \sigma_{AA} = \sigma_{BB}$. The c_i are functions of Δ and x and are of the form

$$c_1 = 3c_3 - 4B_3/B_2^2 \tag{10}$$

$$c_2 = (f_{21} + f_{22}\Delta + f_{23}\Delta^2)\Delta x(1 - x) \tag{11}$$

$$c_3 = 1 + (f_{31} + f_{32}\Delta + f_{33}\Delta^2)\Delta x(1 - x) \tag{12}$$

$$c_4 = (f_{41} + f_{42}\Delta + f_{43}\Delta^2)\Delta x(1 - x) \tag{13}$$

with

$$B_3 = \frac{\pi^2}{18}\sigma^6[5 + \Delta(60 + 78\Delta + 32\alpha^2)x(1 - x)] \tag{14}$$

The constants f_{ij} were determined from Monte Carlo simulation results[47] and are given by

$$f_{21} = 16.583 \quad f_{22} = 227.504 \quad f_{23} = 353.879$$

$$f_{31} = -10.055 \quad f_{32} = -5.794 \quad f_{33} = 14.826$$

$$f_{41} = -1.200 \quad f_{42} = 54.302 \quad f_{43} = 102.365 \tag{15}$$

This equation of state is accurate for nonadditivity parameters $-0.5 \leq \Delta \leq 1$, at any composition ($0 \leq x \leq 1$) and in the range of densities where the homogeneous fluid is stable. Note that for the range of Δ studied here (i.e., $\Delta \leq 0$), no demixing transition occurs in the reference system. Although crystallization at sufficiently high densities is possible, we ignore this possibility in this work.

To obtain the free energy $f_{ref}(\rho,x)$, we numerically integrate the equation of state as a function of density, starting from an ideal-gas reference state:

$$\beta f(\rho, x) = \beta f_{id}(\rho, x) + \int_0^\rho \frac{\beta P(\rho', x) - \rho'}{\rho'^2}\,d\rho' \tag{16}$$

with the ideal gas free energy given by

$$\beta f_{\text{id}}(\rho, x) = \log \rho \Lambda^3 - 1 + x \log x + (1 - x) \log(1 - x) \tag{17}$$

Here Λ is the thermal de Broglie wavelength, which can be chosen equal to σ for simplicity. Note that the last two terms in eq 17 denote the mixing entropy.

To determine the contact value of the pair correlation function $g_{ij}(\sigma_{ij})$ (with $i,j \in \{A,B\}$), we use an approximation proposed by Hamad (see refs 48 and 63). Specifically, we use

$$g_{ij}(\rho, x) = g_{\text{pure}}(\rho \sigma^3 \mathcal{X}_{ij}) \tag{18}$$

with

$$\mathcal{X}_{ij} = \frac{b_2}{b_3} \frac{\sum_k x_k c_{k;ij}}{\sigma^d} \tag{19}$$

Here, $b_2 = 4$ and $b_3 = 10$ are the reduced virial coefficients for a monodisperse hard-sphere fluid, and the sum is taken over $k \in \{A,B\}$. The coefficients $c_{k;ij}$ are given by

$$c_{k;ij} = \sigma_{k;ij}{}^3 + \frac{3}{2} \frac{\sigma_{k;ij}{}^2}{\sigma_{ij}} \sigma_{i;jk} \sigma_{j;ik} \tag{20}$$

$$\sigma_{k;ij} \equiv \sigma_{ik} + \sigma_{jk} - \sigma_{ij} \tag{21}$$

■ AUTHOR INFORMATION

Corresponding Author
*E-mail: f.smallenburg@gmail.com.

Notes
The authors declare no competing financial interest.

■ ACKNOWLEDGMENTS

■ REFERENCES

(1) Poole, P. H.; Sciortino, F.; Essmann, U.; Stanley, H. E. Phase Behaviour Of Metastable Water. *Nature* **1992**, *360*, 324−328.

(2) Holten, V.; Bertrand, C.; Anisimov, M.; Sengers, J. Thermodynamics of Supercooled Water. *J. Chem. Phys.* **2012**, *136*, 094507.

(3) Mishima, O.; Stanley, H. E. The Relationship Between Liquid, Supercooled and Glassy Water. *Nature* **1998**, *396*, 329−335.

(4) Sastry, S.; Angell, C. A. Liquid-liquid Phase Transition in Supercooled Silicon. *Nat. Mater.* **2003**, *2*, 739−743.

(5) Vasisht, V. V.; Saw, S.; Sastry, S. Liquid-Liquid Critical Point in Supercooled Silicon. *Nat. Phys.* **2011**, *7*, 549−553.

(6) Glosli, J. N.; Ree, F. H. Liquid-Liquid Phase Transformation in Carbon. *Phys. Rev. Lett.* **1999**, *82*, 4659−4662.

(7) Beye, M.; Sorgenfrei, F.; Schlotter, W. F.; Wurth, W.; Föhlisch, A. The Liquid-Liquid Phase Transition in Silicon Revealed by Snapshots of Valence Electrons. *Proc. Natl. Acad. Sci. U.S.A.* **2010**, *107*, 16772−16776.

(8) Soper, A. K.; Ricci, M. A. Structures of High-Density and Low-Density Water. *Phys. Rev. Lett.* **2000**, *84*, 2881.

(9) Loerting, T.; Giovambattista, N. Amorphous Ices: Experiments and Numerical Simulations. *J. Phys.: Condens. Matter* **2006**, *18*, R919−R977.

(10) Mishima, O.; Calvert, L.; Whalley, E. An Apparently First-order Transition Between Two Amorphous Phases of Ice Induced by Pressure. *Nature* **1985**, *314*, 76−78.

(11) Amann-Winkel, K.; Gainaru, C.; Handle, P. H.; Seidl, M.; Nelson, H.; Böhmer, R.; Loerting, T. Water's Second Glass Transition. *Proc. Natl. Acad. Sci. U.S.A.* **2013**, *110*, 17720−17725.

(12) Murata, K.; Tanaka, H. Liquid-Liquid Transition Without Macroscopic Phase Separation in a Water-Glycerol Mixture. *Nat. Mater.* **2012**, *11*, 436−443.

(13) Pallares, G.; El Mekki Azouzi, M.; González, M. A.; Aragones, J. L.; Abascal, J. L. F.; Valeriani, C.; Caupin, F. Anomalies in Bulk Supercooled Water at Negative Pressure. *Proc. Natl. Acad. Sci. U.S.A.* **2014**, *111*, 7936−7941.

(14) Debenedetti, P. G. Supercooled and Glassy Water. *J. Phys.: Condens. Matter* **2003**, *15*, R1669.

(15) Kolafa, J.; Nezbeda, I. Monte Carlo Simulations on Primitive Models of Water and Methanol. *Mol. Phys.* **1987**, *61*, 161−175.

(16) De Michele, C.; Gabrielli, S.; Tartaglia, P.; Sciortino, F. Dynamics in the Presence of Attractive Patchy Interactions. *J. Chem. Phys. B* **2006**, *110*, 8064−8079.

(17) Ford, M. H.; Auerbach, S. M.; Monson, P. On The Mechanical Properties and Phase Behavior of Silica: A Simple Model Based on Low Coordination and Strong Association. *J. Chem. Phys.* **2004**, *121*, 8415−8422.

(18) De Michele, C.; Tartaglia, P.; Sciortino, F. Slow Dynamics in a Primitive Tetrahedral Network Model. *J. Chem. Phys.* **2006**, *125*, 204710.

(19) Saika-Voivod, I.; Smallenburg, F.; Sciortino, F. Understanding Tetrahedral Liquids through Patchy Colloids. *J. Chem. Phys.* **2013**, *139*, 234901.

(20) Tu, Y.; Buldyrev, S. V.; Liu, Z.; Fang, H.; Stanley, H. E. Different Water Scenarios for a Primitive Model with Two Types of Hydrogen Bonds. *Europhys. Lett.* **2012**, *97*, 56005.

(21) Smallenburg, F.; Filion, L.; Sciortino, F. Erasing No-Man's Land by Thermodynamically Stabilizing the Liquid-liquid Transition in Tetrahedral Particles. *Nat. Phys.* **2014**, *10*, 653−657.

(22) Noya, E. G.; Vega, C.; Doye, J. P. K.; Louis, A. A. Phase Diagram of Model Anisotropic Particles with Octahedral Symmetry. *J. Chem. Phys.* **2007**, *127*, 054501.

(23) Doye, J. P.; Louis, A. A.; Lin, I.-C.; Allen, L. R.; Noya, E. G.; Wilber, A. W.; Kok, H. C.; Lyus, R. Controlling Crystallization and Its Absence: Proteins, Colloids and Patchy Models. *Phys. Chem. Chem. Phys.* **2007**, *9*, 2197−2205.

(24) Bianchi, E.; Blaak, R.; Likos, C. N. Patchy Colloids: State of the Art and Perspectives. *Phys. Chem. Chem. Phys.* **2011**, *13*, 6397−6410.

(25) Wertheim, M. S. Fluids with Highly Directional Attractive Forces. I. Statistical Thermodynamics. *J. Stat. Phys.* **1984**, *35*, 19−34.

(26) Wertheim, M. S. Fluids with Highly Directional Attractive Forces. II. Thermodynamic Perturbation Theory and Integral Equations. *J. Stat. Phys.* **1984**, *35*, 35−47.

(27) Wertheim, M. S. Fluids with Highly Directional Attractive Forces. III. Multiple Attraction Sites. *J. Stat. Phys.* **1986**, *42*, 459−476.

(28) Sciortino, F.; Bianchi, E.; Douglas, J. F.; Tartaglia, P. Self-Assembly of Patchy Particles into Polymer chains: A Parameter-Free Comparison between Wertheim Theory and Monte Carlo Simulation. *J. Chem. Phys.* **2007**, *126*, 194903.

(29) Smallenburg, F.; Leibler, L.; Sciortino, F. Patchy Particle Model for Vitrimers. *Phys. Rev. Lett.* **2013**, *111*, 188002.

(30) Rovigatti, L.; Bomboi, F.; Sciortino, F. Accurate Phase Diagram of Tetravalent DNA Nanostars. *J. Chem. Phys.* **2014**, *140*, 154903.

(31) Hsu, C. W.; Largo, J.; Sciortino, F.; Starr, F. W. Hierarchies of Networked Phases Induced by Multiple Liquid-Liquid Critical Points. *Proc. Natl. Acad. Sci. U.S.A.* **2008**, *105*, 13711−13715.

(32) Hsu, C. W.; Starr, F. W. Interpenetration as a Mechanism for Liquid-Liquid Phase Transitions. *Phys. Rev. E* **2009**, *79*, 041502.

(33) Starr, F.; Sciortino, F. "Crystal-Clear" Liquid-Liquid Transition in a Tetrahedral Fluid. *Soft Matter* **2014**, DOI: 10.1039/C4SM01835D.

(34) Palmer, J. C.; Martelli, F.; Liu, Y.; Car, R.; Panagiotopoulos, A. Z.; Debenedetti, P. G. Metastable Liquid-Liquid Transition in a Molecular Model of Water. *Nature* **2014**, *510*, 385−388.

(35) Russo, J.; Tanaka, H. Understanding Water's Anomalies with Locally Favored Structures. *Nat. Commun.* **2014**, 3556.

(36) Cuthbertson, M. J.; Poole, P. H. Mixturelike Behavior Near a Liquid-Liquid Phase Transition in Simulations of Supercooled Water. *Phys. Rev. Lett.* **2011**, *106*, 115706.

(37) Holten, V.; Limmer, D. T.; Molinero, V.; Anisimov, M. A. Nature of the Anomalies in the Supercooled Liquid State of the mW Model of Water. *J. Chem. Phys.* **2013**, *138*, 174501.

(38) Holten, V.; Palmer, J. C.; Poole, P. H.; Debenedetti, P. G.; Anisimov, M. A. Two-state Thermodynamics of the ST2 Model for Supercooled Water. *J. Chem. Phys.* **2014**, *140*, 104502.

(39) Sciortino, F. Primitive Models of Patchy Colloidal Particles. A Review. *Collect. Czech. Chem. Commun.* **2010**, *75*, 349−358.

(40) de las Heras, D.; Tavares, J. M.; Telo da Gama, M. M. Phase Diagrams of Binary Mixtures of Patchy Colloids with Distinct Numbers of Patches: the Network Fluid Regime. *Soft Matter* **2011**, *7*, 5615−5626.

(41) Tavares, J. M.; Almarza, N. G.; Telo da Gama, M. M. Three-Dimensional Patchy Lattice Model: Ring Formation and Phase Separation. *J. Chem. Phys.* **2014**, *140*, 044905.

(42) Russo, J.; Tavares, J. M.; Teixeira, P. I. C.; Telo da Gama, M. M.; Sciortino, F. Reentrant Phase Diagram of Network Fluids. *Phys. Rev. Lett.* **2011**, *106*, 085703.

(43) Tavares, J.; Teixeira, P.; Telo da Gama, M. How Patchy Can One Get and Still Condense? The Role of Dissimilar Patches in the Interactions of Colloidal Particles. *Mol. Phys.* **2009**, *107*, 453−466.

(44) Tavares, J. M.; Teixeira, P. I. C.; Telo da Gama, M. M. Criticality of Colloids with Distinct Interaction Patches: The Limits of Linear Chains, Hyperbranched Polymers, and Dimers. *Phys. Rev. E* **2009**, *80*, 021506.

(45) Marshall, B. D.; Chapman, W. G. A Density Functional Theory for Patchy Colloids Based on Wertheim's Association Theory: Beyond the Single Bonding Condition. *J. Chem. Phys.* **2013**, *138*, 044901.

(46) Kern, N.; Frenkel, D. Fluid-Fluid Coexistence in Colloidal Systems with Short-Ranged Strongly Directional Attraction. *J. Chem. Phys.* **2003**, *118*, 9882−9889.

(47) Jung, J.; Jhon, M. S.; Ree, F. H. An Analytic Equation of State and Structural Properties of Nonadditive Hard Sphere Mixtures. *J. Chem. Phys.* **1994**, *100*, 9064.

(48) Hamad, E. Z. A General Mixture Theory. I. Mixtures of Spherical Molecules. *J. Chem. Phys.* **1996**, *105*, 3229−3234.

(49) Franzese, G.; Malescio, G.; Skibinsky, A.; Buldyrev, S. V.; Stanley, H. Generic Mechanism for Generating a Liquid-Liquid Phase Transition. *Nature* **2001**, *409*, 692−695.

(50) Sciortino, F.; Giacometti, A.; Pastore, G. Phase Diagram of Janus Particles. *Phys. Rev. Lett.* **2009**, *103*, 237801.

(51) Binder, K.; Landau, D. Phase Diagrams and Critical Behavior in Ising Square Lattices with Nearest-and Next-Nearest-Neighbor Interactions. *Phys. Rev. B* **1980**, *21*, 1941.

(52) Tavares, J.; da Gama, M. T.; Teixeira, P.; Weis, J.; Nijmeijer, M. Phase Diagram and Critical Behavior of the Ferromagnetic Heisenberg Fluid from Density-Functional Theory. *Phys. Rev. E* **1995**, *52*, 1915.

(53) Weis, J.; Nijmeijer, M.; Tavares, J.; da Gama, M. T. Phase Diagram of Heisenberg Fluids: Computer Simulation and Density Functional Theory. *Phys. Rev. E* **1997**, *55*, 436−446.

(54) Köfinger, J.; Wilding, N. B.; Kahl, G. Phase Behavior of a Symmetrical Binary Fluid Mixture. *J. Chem. Phys.* **2006**, *125*, 234503.

(55) Wilding, N. B.; Schmid, F.; Nielaba, P. Liquid-Vapor Phase Behavior of a Symmetrical Binary Fluid Mixture. *Phys. Rev. E* **1998**, *58*, 2201−2212.

(56) Pini, D.; Tau, M.; Parola, A.; Reatto, L. Phase Diagram of Symmetric Binary Mixtures at Equimolar and Nonequimolar Concentrations: A Systematic Investigation. *Phys. Rev. E* **2003**, *67*, 046116.

(57) Dorsaz, N.; Foffi, G. Phase Behaviour of the Symmetric Binary Mixture from Thermodynamic Perturbation Theory. *J. Phys.: Condens. Matter* **2010**, *22*, 104113.

(58) Xu, L.; Kumar, P.; Buldyrev, S. V.; Chen, S.-H.; Poole, P. H.; Sciortino, F.; Stanley, H. E. Relation Between the Widom Line and the Dynamic Crossover in Systems with a Liquid-liquid Phase Transition. *Proc. Natl. Acad. Sci. U.S.A.* **2005**, *102*, 16558−16562.

(59) Poole, P. H.; Saika-Voivod, I.; Sciortino, F. Density Minimum and Liquid-Liquid Phase Transition. *J. Phys.: Condens. Matter* **2005**, *17*, L431.

(60) Holten, V.; Anisimov, M. Entropy-Driven Liquid-Liquid Separation in Supercooled Water. *Sci. Rep.* **2012**, *2*, 713.

(61) Brazhkin, V.; Fomin, Y.; Ryzhov, V.; Tareyeva, E.; Tsiok, E. True Widom Line for a Square-Well System. *Phys. Rev. E* **2014**, *89*, 042136.

(62) Sciortino, F.; Saika-Voivod, I.; Poole, P. H. Study of the ST2 Model of Water Close to the Liquid-Liquid Critical Point. *Phys. Chem. Chem. Phys.* **2011**, *13*, 19759−19764.

(63) Santos, A.; De Haro, M. L.; Yuste, S. Equation of State of Nonadditive d-Dimensional Hard-Sphere Mixtures. *J. Chem. Phys.* **2005**, *122*, 024514.

H

dx.doi.org/10.1021/jp508788m | *J. Phys. Chem. B* XXXX, XXX, XXX−XXX